Ocean Dynamics (2016) 66:119–132
DOI 10.1007/s10236-015-0913-z

Monitoring tidal currents with a towed ADCP system

Alexei Sentchev[1] · **Max Yaremchuk**[2]

Received: 22 September 2015 / Accepted: 10 December 2015 / Published online: 22 December 2015

Abstract The tidal circulation in the semi-enclosed Boulogne harbour (eastern English Channel) is measured during the various stages of the tidal cycle with a low-cost towed Acoustic Doppler Current Profiler (ADCP) system for the first time. The system is equipped with an interpolation algorithm which allows reconstructing space-time evolution of the velocity field for surveys whose duration is comparable or larger than the typical time of tidal variation (1–2 h). The method employs space-time velocity covariances derived from a numerical simulation of the surveyed area by a high-resolution relocatable model "Model for Applications on Regional Scale" (MARS). The covariances are utilized by the optimal interpolation algorithm to obtain the most likely evolution of the velocity field under the constraints provided by the ADCP observations and their error statistics. Technically, the MARS model run provides the first guess (background) evolution of the velocity field in the surveyed area which is then corrected by the data in a statistically consistent manner as it explicitly takes into the account both observational and modeling errors. The quality of the velocity reconstruction was validated against independent bottom-mounted ADCP data, the background model evolution, and against the results of spatial interpolation by Kriging technique. All tests demonstrated significant (30 to 60 %) reduction of the model-data misfit for the velocity field obtained as a result of space-time optimal interpolation. Although the method was applied to recover surface circulation, it can be extended for assessment of the full 4D tidal flow dynamics using the data recorded throughout the entire water column.

Keywords Towed ADCP survey · Tidal currents · English Channel · Optimal interpolation

Responsible Editor: Alexander Barth

This article is part of the Topical Collection on the *47th International Liège Colloquium on Ocean Dynamics, Liège, Belgium, 4-8 May 2015*

✉ Alexei Sentchev
Alexei.Sentchev@univ-littoral.fr

Max Yaremchuk
max.yaremchuk@nrlssc.navy.mil

[1] University of Littoral - Côte d'Opale, CNRS, Univ. Lille, UMR 8187 LOG, Laboratoire d'Océanologie et de Géosciences, F 59000 Lille, France

[2] Naval Research Laboratory, Stennis Space Center, Bldg. 1009, Mississippi, MS 39529, USA

1 Introduction

In recent years, assessing marine renewable energy potential became a hot topic in many branches of applied research. Tidal stream energy conversion (using an in-stream turbine) is becoming an increasingly favored form of renewable energy due to the predictable periodicity of the tide, high energy density, and nearshore resource location. All these make tidal stream energy a more reliable source than other forms of marine energy, such as waves and offshore wind. The place of tidal stream energy conversion in a future energy generation mix is under evaluation in different countries (e.g., Weisberg et al. 2012; Quirapas et al. 2015).

In coastal ocean, the most promising sites have limited size and are located near the shore (straits, passage between islands, or areas close to headlands). Here, the theoretical potential varies from 0.01 to 1 GW (e.g., Haas et al. 2011), and the site screening is an essential first step towards successful selection of technology and devices to be deployed. However, site selection is not simply a case of identifying areas with strong tidal currents. Resource assessment should consider a

wide range of factors, including temporal and spatial variability of the major parameters of the flow (e.g., Neill et al. 2014). Therefore, tidal stream resource assessments typically make extensive use of validated hydrodynamic models (e.g., Blunden and Bahaj 2006; Goddijn-Murphy et al. 2013; Lewis et al. 2015). But it is not sufficient, and detailed observations are required for estimating and mapping the tidal flow parameters at high space and time resolution. Most of the oceanographic surveys devoted to renewable energy site assessment employ vessel-mounted Acoustic Doppler Current Profiler (ADCP) as a tool. In contrast to the bottom-mounted ADCPs, this method of surveying does not require deployment of numerous instruments (ADCPs) to obtain adequate spatial resolution and is not vulnerable to harsh environmental conditions imposed by the extreme tidal velocities either.

Vessel-mounted ADCPs were used to measure tidal currents for more than two decades (e.g., Geyer and Signell 1990; Simpson et al. 1990; Vennell 1994). While the vessel steams around a circuit, velocity profiles are recorded with sufficient frequency to resolve spatial irregularities of the flow field. In these early studies, the spatial resolution of reconstructed current maps attained 500 m. Old and Vennell (2001) exploited the improved accuracy of "broadband" ADCP to achieve much better horizontal resolution (20 m across the flow and 150 m along the flow) providing a detailed view of the 2D structure of an ebb-tidal jet. The temporal variation of the flow was accounted for using simple harmonic representation. Gooch et al. (2009) also used only spatial (along-isobath) interpolation technique neglecting the tidal phase difference during the smaller-scale (500 m) ADCP surveys accomplished in approximately 30 min. This approach could be useful for the assessment of relatively small sites, but still requires velocity monitoring during multiple stages of the tidal cycle. Vennell (2006) used a biharmonic spline tidal analysis technique, proposed by Candela et al. (1992), for space-time interpolation of velocity data recorded by an ADCP in a narrow (600-m wide) tidal channel. This study revealed high sensitivity of the method to the amount of data and their spatial distribution. Later on, Vennell and Beatson (2006, 2009) developed a 2D divergence-free spatial interpolator for depth-averaged tidal velocities. The method uses the continuity constraint, ensures mass conservation, and provides more realistic estimates for the depth-averaged velocity field. MacMahan et al. (2012) applied similar technique for interpolating noisy data from an ADCP mounted on the underwater vehicle.

It is well established now that, at pilot sites, the power generating potential of the tidal stream is characterized by significant variations at the scales of a few hundred meters (Li 2006; Goddijn-Murphy et al. 2013) and thus requires very high resolution surveying during multiple tidal cycles. At the same time, the accuracy in reconstruction of the full 4D tidal flow can be significantly increased by merging observed velocities with the dynamical constraints provided by the numerical models. This approach was pursued by Goddijn-Murphy et al. (2013), who synthesized vessel-mounted ADCP transects in the Pentland Firth (Scotland) with the output of the Orkney 2D tidal Model (ORKM) at 1 km resolution. Their method employed spatial interpolation of the model-derived velocity variations onto the observation points to "synchronize in time" the surveyed velocities. The latter were spatially interpolated onto the fine (150 m resolution) grid to obtain snapshots of the currents during different tidal phases.

In this work, we present a technique for interpolating underway velocity measurements in space and time and report the method's performance. In atmospheric and ocean sciences, the conventional name of the method is optimal interpolation (OI). In our case, recorded velocities are synchronized in time using the output statistics from the regional model (Model for Applications on Regional Scale (MARS)-3D) configured for high-resolution simulations in the surveyed area. Since the synchronization algorithm is based on the optimal interpolation of the data, recorded observations can be naturally projected on a regular space-time grid consistent with the survey's resolution to obtain the full time evolution of the velocity fields in the area. The consistency between the space-time resolution of observations and model configuration is the first valuable advantage of the method. The second advantage is its capability to provide statistical estimates of the accuracy of reconstructed velocity field at every time step. The OI technique has more than 60-year history of application in environmental sciences, and as it has been demonstrated by many authors (e.g., Bretherton et al. 1976; Thiébaux and Pedder 1987; Wunsch 1996), the method is pretty robust and easy to implement. In the considered application, the background error statistics is derived from the output of a regional circulation model. The approach does not require knowledge of the model forecast skill mandatory for the implementation of more advanced data assimilation techniques (e.g., Kalnay 2002; Barth et al. 2009).

In the present study, we applied the OI technique to underway measurements recorded by a towed (not vessel-mounted) ADCP and report the performance of a new towed ADCP system, capable of tidal current surveying at towing speeds up to 4 m/s. In addition to the standard ADCP preprocessing software, the system is equipped with a filter which removes the GPS positioning errors.

The system has been tested in the Boulogne harbour (La Manche). This region was elected for several reasons. First, due to its very big tidal range (9 m), relatively strong (2 m/s) currents, and moderate wind waves (less than 3 m in the annual mean), it is considered to be a prospective place for the development and testing of the various prototypes of tidal energy conversion (TEC) devices. Second, there is a strong necessity to monitor and control the Boulogne harbour environment which is affected by the agricultural runoff and

pollution by local industries. Finally, there is a growing demand of accurate low-cost estimation of tidal currents at the prospective sites for tidal power generation. The presented system (towed instrumented platform and data processing software) was developed in response to these needs and may prove to be useful in many other coastal applications which require monitoring coastal environments and tidal circulation.

2 Measurements

2.1 Study site

The measurements presented here were made in the Boulogne harbour (BLH) located in the Strait of Dover (eastern English Channel) (Fig. 1, left panel). The surveyed area is approximately 2 × 2 km square with a shallow beach in the East, and a 4–8-m deep fairway crossing the domain in the South (Fig. 1, middle panel). The average depth of the basin is 5.4 m (at the lowest spring tide), around 8 m in the West, rapidly increasing seaward. The 0 m isobath delimits the shallow eastern part with a large drying beach. Surface elevation in the BH exhibits strong (up to 9 m) variations depending on the stage of the tide. The local tide is characterized by the predominant semi-diurnal period, small diurnal inequality, and fortnightly modulation due to the interference of the major semi-diurnal (M_2, S_2, N_2) constituents. The asymmetry of sea level variation, caused by overtides, implies that the duration of falling tide exceeds that of the rising tide by approximately 2 h with stronger currents occurring during flood flow. A prominent feature of tidal circulation in the harbour is a large anticyclonic eddy driven by the strong northward flow outside the BLH during the rising tide (Fig. 1, right panel). Although the existence of the eddy is well known for navigators, its temporal variability and the circulation pattern during the ebb flow have not been quantified in detail.

Strong tidal forcing induces vertical mixing throughout the water column in the majority of the domain. Circulation in the harbour can be also affected by the discharge of the Liane river whose transport is regulated by a number of tidal gates. When the gates are open, the peak discharge may reach 10^6 m^3/day, which is quite significant given the small water volume (3×10^7 m^3) in the harbour.

2.2 Measurement system

High-resolution current mapping was performed in the BLH using an experimental platform carrying a broadband ADCP (1200 kHz Teledyne RDI WorkHorse Sentinel) towed by a light boat (zodiac). The platform, featuring two cylindrical hulls 1.80 m long and 0.22 m in diameter, connected by a 0.8 × 0.8-m stainless frame, is able to carry other instruments, such as mini CTD, ADV (Fig. 2). The distance from the boat is controlled by an adjustable side fin allowing to avoid contamination by the wake of the boat. Two additional rear fins installed on the hulls assure stability of the forward propulsion. The ADCP's transducer head is located roughly 0.2 m below the water surface with the third beam aligned along the platform's centreline. In the test runs, the blanking was set to 0.3 m, the bin size to 0.5 m, and the center of the first bin was roughly at 0.75 m. The velocity profiles were obtained throughout the entire water column. The ADCP was set to operate at the pinging rate of 1 Hz. Velocity profiling was carried out within 1-s interval. Each ping for velocity was composed of three sub-pings averaged within 1-s interval, providing velocity error of 0.04 m/s. Single-ping bottom tracking was enabled to correct for boat's movement, and the recorded velocities formed a current vector in the fixed frame relative to the bottom.

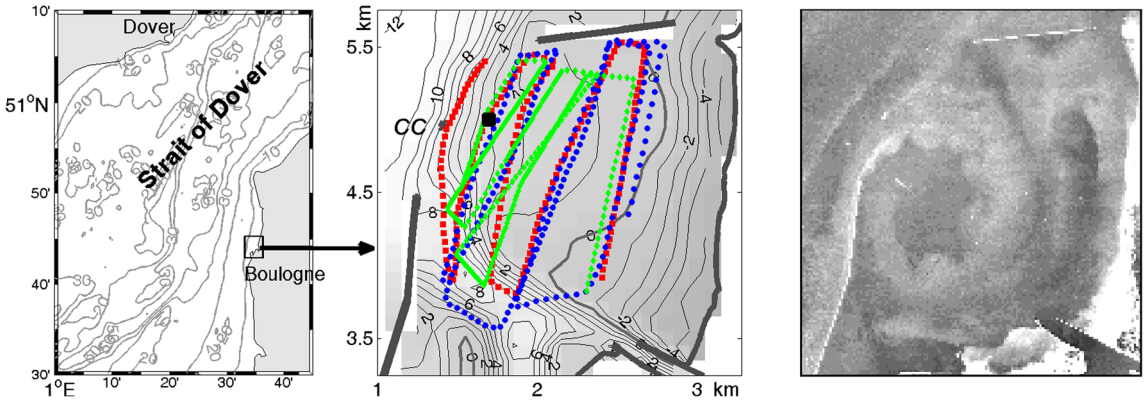

Fig. 1 *Left panel*: Map of the Strait of Dover with bathymetry (m) and location of the Boulogne harbour. *Middle*: Map of the Boulogne harbour with bathymetry (m) and three successive surveys: 1200-1400GMT on March 27, 2012 (*green*), 0700-0825GMT on March 29, 2012 (*red*), and 1740-1920GMT on June 28, 2012 (*blue*). Location of the bottom-mounted ADCP is shown by the *black square*, 250 m east of the concrete caisson (*CC*). *Right*: aerial snapshot of the Boulogne harbour during the flood flow, HW−1 h. An anticyclonic eddy centered 400 m east of the western dyke is clearly seen

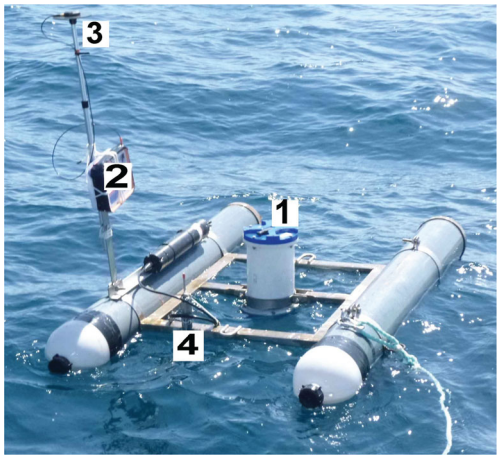

Fig. 2 The experimental towing platform with (*1*) ADCP profiler, (*2*) high-precision GPS and data acquisition module, (*3*) GPS antenna, (4) Acoustic Doppler Velocimeter (ADV)

The boat speed was varied during the surveys in the range within 2 to 5 m/s for the majority of the tracks. Higher towing speed (4–5 m/s) was occasionally chosen to test the limits of the system's ability of velocity profiling. The recorded ADCP data were merged with high-resolution GPS data. The geolocalisation system GENEQ SXblue was mounted on the left side of the platform (Fig. 2) and operated at 1 Hz, providing the nominal positioning accuracy better than 1 m.

2.3 Towed ADCP surveys

Three surveys were performed to assess the circulation pattern in BLH and to test the system in operation. Their tracks are shown in the middle panel of Fig. 1. The first survey was made on March 27, 2012 at 12–14 UTC, during the flood tide (HW-1.5 h to HW+0.5 h). The second survey took place 2 days later, on March 29. It was targeted at monitoring the currents during the ebb flow and lasted slightly less than 1.5 h from LW-2.3 to LW-1 h. The third, 1.7-h survey, was performed on the 28th of June 2012 between HW + 0.3 and HW + 2 h.

The transects were oriented roughly in the meridional direction and were separated by 200–300 m (Fig. 1, middle panel). During the third survey, a couple of tracks were repeated twice at different towing speeds with an objective to evaluate the impact of towing velocity on the system's performance.

Current velocities throughout the water column were corrected for boat motion, using both bottom-tracking and GPS coordinates available at 1-s resolution, and then smoothed by the Gaussian-shaped running window with the half-width τ of 15 s. The filter removes variability on spatial scales of $2v\boldsymbol{\tau}$ (v is the towing speed). After that, the velocities were subsampled every 30 s, so that separations between the thinned along-track data points varied within 60–100 m, depending on the towing speed.

Figure 3 shows northward velocity time series recorded in the surface layer during the third survey along two tracks in the eastern part of the BLH, 1 h after the HW. Significant variability of the velocity on various time scales is observed. The respective velocity spectra (not shown) are rather noisy with a slight dominance of velocity fluctuations at 6–8-s periods, probably caused by the effect of surface waves. The intensity of velocity fluctuations, normalized by the mean velocity magnitude, ranges from 1.6 for northward track to 0.9 for southward track (Fig. 3). Lower variability was typically observed at higher towing speeds (3.5–4 m/s) and when towing along the waves (track 6 in Fig. 3). Similar variability has been observed in the records of the along-track coordinates. After filtering the velocity and coordinate values, the typical towing speed was nearly constant, ranging within 2–2.5 m/s (4–5 m/s for fast surveying), and the velocity values did not show any variations at spatial scales below 200 m.

3 Optimal interpolation of velocity measurements

3.1 Basic formulation

Towed ADCP measurements from repeated tracks contain information on both spatial and temporal variations of tidal currents, and a number of techniques have been used to separate these variations. Some of them use harmonic representation of velocity evolution. This approach brings artificial disturbances into the spatial structure of velocity field while methods based on biharmonic splines impose spatial smoothness of the interpolated field, which is a reasonable choice for many applications where temporal variability could be neglected. A short review of the interpolation methods for tidal velocity surveying has been done by Vennell (2006). More recent approach, aiming to preserve the dynamically consistent structure of the flow (i.e., the physics of tidal motion), utilizes a numerical model for velocity interpolation (e.g., Goddijn-Murphy et al. 2013).

A straightforward way of constrained spatial interpolation of a vector field is the well-known method of optimal interpolation (OI) pioneered by Gandin (1963). Since then, the approach was widely adopted in geosciences (e.g., Bretherton et al. 1976; Thiébaux and Pedder 1987). The OI technique can be easily extended to include time dimension by using the space-time correlation functions. In this approach, the optimal correction to the evolution of a background vector field $\boldsymbol{u}^m(\boldsymbol{x},t)$ defined on a regular (model) grid is represented by a linear combination of the weighted differences between the background model trajectory and the observed velocities. The weights a_i are chosen so as to minimize the mean square difference between observations $\boldsymbol{u}_i^*$ and the background field values $\boldsymbol{u}^m$, interpolated into the space-time locations of the observations by the (linear) operator $\boldsymbol{H}^i$, projecting gridded

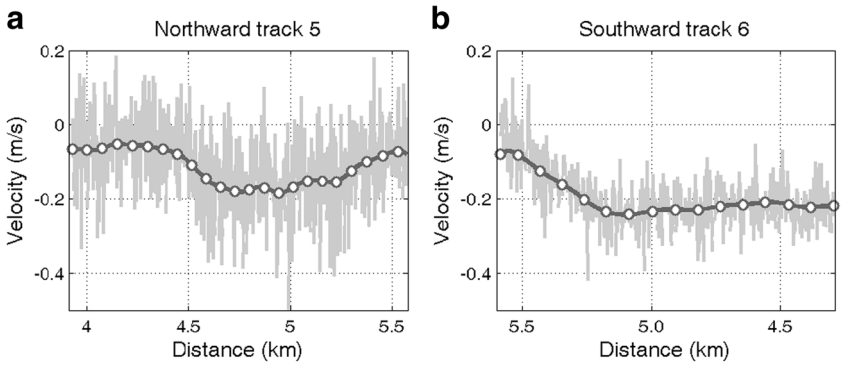

Fig. 3 An example of two ADCP records acquired along two transects at the end of the third survey. Original record of the northward velocity is shown by the *spiky gray line*. *Solid line* shows filtered data. *White circles* show velocity values used for data interpolation in space and time

velocity values onto the *i*th observation point from the apexes of the enveloping grid cell:

$$J_u = \left\langle \left[\boldsymbol{u}^m + \sum\nolimits_i a_i \left(\boldsymbol{H}^i \boldsymbol{u}^m - \boldsymbol{u}_i^* \right) \right]^2 \right\rangle \rightarrow \min(a_i). \qquad (1)$$

Here, angular brackets denote the statistical (ensemble) average, and summation is made over all (distributed in space and time) the velocity values measured during the survey period. Given the space-time covariance matrices of the model $\boldsymbol{B} = \langle \boldsymbol{u}^m(\boldsymbol{x},t)\boldsymbol{u}^m(\boldsymbol{x}',t') \rangle$ and observations $\boldsymbol{R}_{ij} = \langle \boldsymbol{u}_i^* \boldsymbol{u}_j^* \rangle$, and assuming that observation errors are not correlated with the model (background) errors, the OI interpolation formula takes the form:

$$\boldsymbol{u}_{opt} = \sum\nolimits_{ij} \boldsymbol{B}\boldsymbol{H}_j^T \left(\boldsymbol{H}_i \boldsymbol{B} \boldsymbol{H}_j^T + \boldsymbol{R}_{ij} \right)^{-1} \left(\boldsymbol{H}^i \boldsymbol{u}^m - \boldsymbol{u}_i^* \right). \qquad (2)$$

In most applications (as well as in the present study), the observation error covariance is assumed to be diagonal. In the considered case, the diagonal values of $\boldsymbol{R}$ are equal to the variances of the along track velocity samples taken at 30-s intervals. The OI takes explicit account of the expected spatial structure of both model and observational errors to produce the velocity field with the least error variance (in a way as to most effectively remove the impact of noise with prescribed space-time structure). More than 50-year history of the application of the OI, the theoretical basis, and a huge amount of publications state that it is a robust interpolator of the noisy data (see for example Wunsch (1996) for more ample discussion). In order to apply Eq. (2) to the velocity surveys, one has to specify the algorithms for computing $\boldsymbol{u}^m(\boldsymbol{x},t)$ and $\boldsymbol{B}$.

3.2 Numerical model and computation of the model error covariances

In the present study, the estimation of the sea state was based on the hydrodynamic model MARS-3D (Lazure and Dumas 2008). The model was configured at 140-m horizontal resolution with 20 sigma levels, vertically distributed such as to provide enhanced resolution near the surface and seabed. Forcing at the open boundaries was taken from a coarser resolution (1 km) model of the English Channel driven by the realistic winds, heat fluxes, and river runoff. The model employs a time-varying spatial grid in the vicinity of the coastline thus taking into account the wetting and drying phenomenon (Plus et al. 2009). The time step of 30 s for both external and internal modes was used. Regional model validation was done by comparing model fields with tidal gage data in 20 ports, sea surface currents recorded by VHF radars, and velocity profiles recorded by a bottom-mounted ADCP deployed in front of the BLH in 2009. More details on the model configuration and validation can be found in Jouanneau et al. (2013). Both coarse (1 km) and fine (0.14 km) resolution models were run for two 35-day periods, in March and June 2012, to simulate currents during the survey periods and to acquire statistics of the current variability. Each coarse resolution model run was preceded by spin-up run. The output velocities from the high-resolution model were interpolated from sigma to z vertical levels with 0.5-m spacing, averaged within a surface layer of 2-m thick, and used for computation of the fine-resolution model error covariance $\boldsymbol{B}$.

In the present study, we used the 7.5-day model run containing 14 2-h periods corresponding to tidal stage of survey 1. For two other surveys, we used other periods specified in Table 1. Each 2-h model trajectory, sampled at 30 s resolution, constitutes an ensemble member. The background model trajectories $\boldsymbol{u}^{\mathrm{m}}(\boldsymbol{x},t)$ corresponding to the surveys were obtained by averaging over the respective 14 2-h periods (i.e., ensemble members are separated by one tidal period). In a similar manner, the space-time background covariance matrix $\boldsymbol{B}$ was computed by averaging over the same 14 ensemble members extracted from the 7.5-day model runs when the modeled tide was exactly in sync with the one observed during the corresponding survey (Fig. 4). Thus, the background covariance matrix is not homogeneous in space and time and is rank deficient. To improve the accuracy in estimating $\boldsymbol{B}$, the matrix elements were localized using the standard localization technique (Hamill et al. 2001) with isotropic Gaussian-shaped localization function. Its half widths (localization scales) in the horizontal $L = 1$ km and temporal $L_\tau = 6$ h directions were

Table 1 Number of the observation points N, mean kinetic energies diagnosed from the surveys KE_{obs} and the respective model runs KE_{mod}, estimated observation and modeling errors, and misfits e between the observed and modeled, e_{mod}, and observed and interpolated, e_{int}, velocities

Survey	N	KE_{obs} (m^2/s^2)	KE_{mod} (m^2/s^2)	Obs. error (m/s)	Mod. error (m/s)	e_{mod}	e_{int}
Mar 27, 1200-1400GMT HW-1.5 h–HW+0.5 h	240	0.076	0.061	0.13	0.12	0.44	0.23
Mar 29, 0700-0825GMT LW-2.3 h–LW-1 h	170	0.023	0.028	0.07	0.10	0.67	0.33
Jun 28, 1740-1920GMT HW+0.3–HW+2 h	200	0.045	0.034	0.15	0.11	0.52	0.14

established in series of numerical experiments. The obtained space-time covariances appeared to capture the dynamical structure of the error fields reasonably well due to the strongly periodic nature of the tide.

The computation of $\boldsymbol{B}$ was performed three times, one time for one particular survey. The interpolation grid adopted for all three surveys contained $n = 10 \times 15$ grid points covering the interior of the harbour (Fig. 5). Estimation of $\boldsymbol{B}$ was one of the most time-consuming parts of the algorithm. However, given a relatively small size of the domain (150 grid points in horizontal, $n_t = 170$–240 observations in time) explicit computation of all the elements of $\boldsymbol{B}$ required by Eq. (2) was performed for each survey.

In this study, we focus on the assessment of the surface circulation in the BLH. For this reason, only velocities in the layer extending from 0.5 to 1.5 m below the sea surface were processed. We did not attempt representing velocity profiles nor depth averaged velocities, relegating this issue for later research.

The overall interpolation quality was quantified in two ways: by estimating the mean relative difference with the data:

$$e = \left[\sum\nolimits_i \left(H_i u^m - u_i^*\right)^2 \Big/ \sum\nolimits_i \left(u_i^*\right)^2\right]^{1/2}, \tag{3}$$

and by calculating the mean interpolation error field $\sigma(\boldsymbol{x})$ which was assessed for each survey by time averaging of the diagonal elements of a posteriori error covariance matrix:

$$\sigma^2(\boldsymbol{x}) = \left\langle \mathrm{diag}\left[\boldsymbol{B}\text{-}\boldsymbol{B}\boldsymbol{H}^T\left(\boldsymbol{H}\boldsymbol{B}\boldsymbol{H}^T + \boldsymbol{R}\right)^{-1}\boldsymbol{H}\boldsymbol{B}\right]\right\rangle. \tag{4}$$

Here, $\boldsymbol{H}$ stands for the $nn_t \times n_t$ matrix whose ith row is given by the nn_t components of $\boldsymbol{H}_{i.}$, and $< >$ denotes time average.

3.3 Tidal circulation in BLH: observed and simulated velocities

Model simulations showed that the tidal circulation inside the BH is not strong, with maximum current velocity of the order of 0.5 m/s, observed in the northern sector of the harbour, and spatially averaged velocity of the order of 0.2 m/s at mean tide (Fig. 4). During rising tide, a large anticyclonic eddy, driven by the strong (1–1.5 m/s) northward flow outside the harbour, is formed at HW-2 h. This transient eddy moves northward and disappears at HW+3 h. During the falling tide, the seaward flow has the highest velocity of 4 h after the HW and the lowest velocity shortly after the LW (Fig. 4). Shallow topography at the extensive eastern beach area strongly affects the ebb flow through frictional effects.

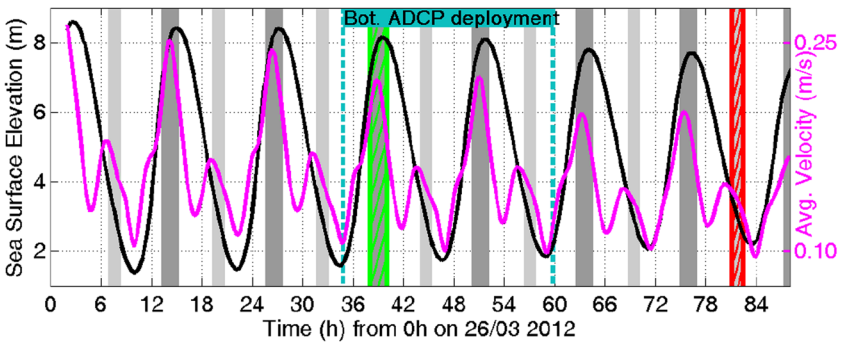

Fig. 4 Time series of the model-derived spatially averaged SSH (*black*) and surface velocity magnitude (*magenta*) during the first 3.5 days of the model run. *Hatched areas* show the periods of towed ADCP surveys: on March 27 (*green*), close to HW, and on March 29 (*red*), close to LW in Boulogne. *Gray shading* shows model ensemble members used for the estimation of velocity covariances: *darker shading* and *green* hatching for the survey 1 (HW), *light gray* shading and *red* hatching for survey 2 (LW). The period of the bottom-mounted ADCP deployment on March 27–28 is shown by *vertical dashed lines* between hours 35 and 60

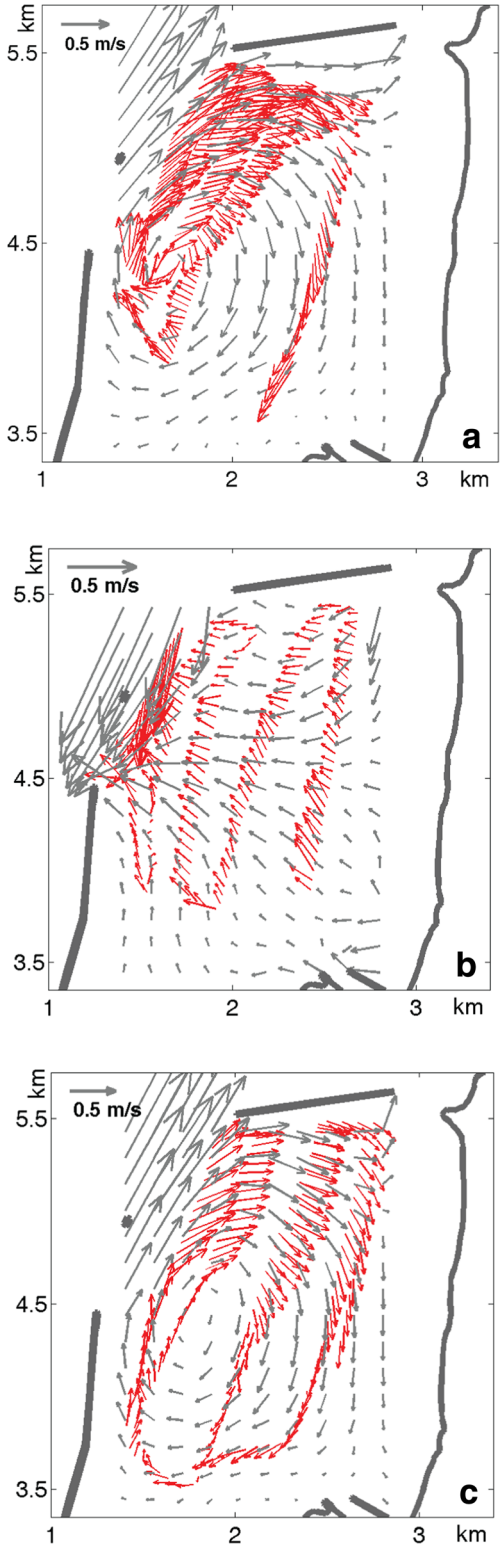

Fig. 5 Observed (*red arrows*) and modeled (*gray arrows*) velocity fields during the first (**a**), second (**b**), and third (**c**) surveys. Model velocities are taken at mid time of each survey

Vector maps of the observed and modeled velocities are shown in Fig. 5 for three particular stages of the tide corresponding to the mid times of the surveys. Vertically averaged observations, sampled at 0.75, 1.25, and 1.75 m, are plotted in Fig. 5 by red arrows for comparison.

The mid-time snapshots of model fields for each survey provide a general view of the consistency between the data and the model before interpolation. Visual inspection reveals significant differences in current speed and direction which apparently depend on horizontal coordinates and tidal stage. In particular, a certain underestimation of the velocity field by the model is found in the southern and eastern parts of the harbour. The discrepancy probably comes from improper model representation of the sandy bottom. Quantitatively, the respective values of e (Eq. 3) varied within 0.44–0.67 (seventh column of Table 1). Such a large misfit can be partly attributed to the abovementioned underestimation of the current velocities by the model (surveys 1 and 3), or their overestimation (survey 2), which is quantitatively visible from comparison of overall kinetic energy values (columns 3 and 4 of Table 1).

Qualitative inspection of Fig. 5 also indicates the necessity of space-time interpolation of the survey data. As an example, a large convergence in the surveyed velocity field is observed ~300 m east of the western dyke in the southern part of the domain during first survey (Fig. 5a). Even larger convergence is visible at the harbour entrance during the second survey (upper left corner in Fig. 5b). On the contrary, the model fields never exhibit such large convergences. We attribute this phenomenon to a relatively large time (20 min) between the respective observations at successive transects: the direction of the relatively weak flow in Fig. 5b does change in approximately half an hour, as the tidal currents reorganize from the inflowing into the outflowing pattern. Similarly, the difference in current direction in the southern sector of the harbour (Fig. 5a) is related to the northward eddy displacement during the flood flow. As it will be shown in the next section, this spurious feature could be eliminated by proper space-time interpolation.

3.4 Space-time interpolation of velocities

The end goal of surveying is to provide an estimate of the velocity field evolution in the area. For a single survey, this is not straightforward due to the temporal evolution of tidal flow. If the surveying time t_s is comparable with the characteristic time scale T of the velocity field, the data have to be interpolated not only in space but in time as well. In the regions dominated by tidal dynamics (T~2–4 h), the latter situation (t_s~T) occurs if surveying is done at the typical speed of a few meters per second, and the surveyed area is larger than a few hundred meters, which is the case in most situations. Goddijn-Murphy et al. (2013) employed a simple interpolation technique to synchronize 2–3-h long surveys at the central reference time using the output of a numerical model. The

synchronized data were then interpolated in space to produce the desired distribution of the velocity field on a regular grid. The presented system is supported by a more general model-based algorithm which utilizes information on space-time correlations between the tidal currents constrained by topography, continuity, stratification, and tidal forcing at the boundaries. The proposed algorithm is capable of estimating the flow field properties at any moment of the survey and providing the corresponding error fields.

Figure 6 gives an example of the interpolated velocity patterns at the mid times: HW-0.5, LW-1.7 and HW+1 h, for the first, second, and third surveys, respectively. The respective observations were projected to the mid time by the OI method, i.e., using space-time correlations provided by the model for the tidal stages corresponding to the surveying periods. The interpolated fields do not contain spurious convergences or divergences of the type seen in Fig. 5a, b and vary smoothly in both space and time. However, the overall agreement between the modeled and interpolated fields varies depending on the number of observations, their space-time distribution, and the model's capability to correctly reproduce tidal phasing and fine scale features of the circulation. Overall, the best agreement is achieved for survey 3, the worst for survey 2. These conclusions are supported by the estimates of the model-data misfits e_{mod} and differences in the mean kinetic energy (cf. columns 3, 4, and 7, 8 in Table 1). A prominent feature of tidal circulation in the BH at rising tide—the clockwise rotating transient eddy—was successfully reconstructed by both surveys (Fig. 6a, c).

To assess the interpolating skill of the OI method, we performed spatial interpolation of velocities sampled during the survey 1 using Kriging technique (Holdaway 1996) with isotropic Gaussian weighting function. Since the weights do not account for time evolution, the interpolated field is could be assumed to represent velocity distribution at the mid time of the survey.

The results of both interpolating techniques are summarized in Fig. 7. The interpolation error $e_i = \boldsymbol{H}_i\boldsymbol{u} - \boldsymbol{u}^*_i$ at the measurement points (Fig. 7c, d) shows much larger fluctuations for Kriging technique with an averaged absolute error value $e = 0.15$ m/s for the meridional velocity component, chosen for comparison. The average misfit is lower for the OI method ($e = 0.09$ m/s) which provides a 50 % gain in accuracy due to taking into account time evolution of the current field.

Another evident advantage of the OI is its capability to fill the entire space of the harbour with interpolated data, whereas Kriging technique provides somewhat less realistic results especially at the periphery of the domain (Fig. 7b). Moreover, comparison shows (Fig. 7) that Kriging and OI provide quite different results in reconstructing the key circulation feature (anticyclonic eddy) during the flood flow. Location of the eddy's center provided by Kriging method is somewhat 200–300 m north of its real position diagnosed by OI and seen in Fig. 1 (right panel). The overall relative error of interpolation is notably larger for the Kriging technique ($e_{\mathrm{int}} = 0.35$) compared to OI ($e_{\mathrm{int}} = 0.23$, Table 1, column 8).

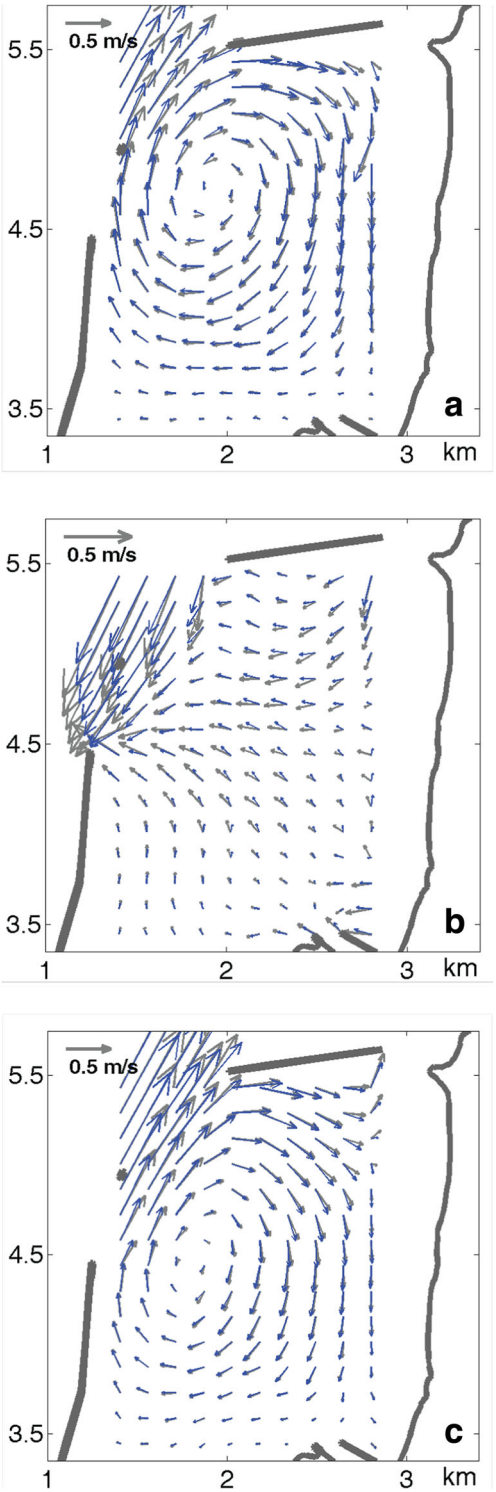

Fig. 6 Velocity fields (*blue arrows*) derived from the survey data by space-time interpolation using model velocities (*gray*) for estimation of the spatio-temporal correlations. The interpolated and model fields are shown for the mid time of the first (**a**), second (**b**), and third (**c**) surveys

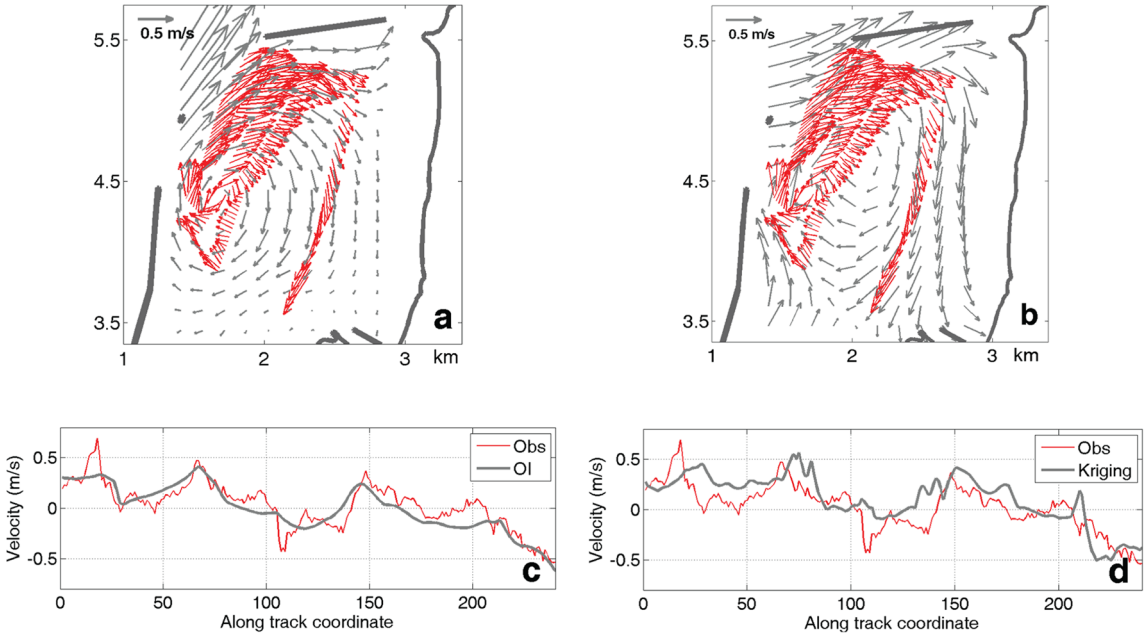

Fig. 7 The interpolated (*gray*) and observed velocity fields (*red*) during the first survey (1200-1400GMT, March 27, 2012). OI interpolation of the data for the mid time of the survey (**a**) and results of interpolation using Kriging technique (**b**). Meridional velocity component of the interpolated fields projected at measurement points (*gray line*) and observed velocity component (*red line*) are shown for each interpolation method below the respective panels (**c**, **d**)

The space-time interpolation also allows tracking the motion of the anticyclonic eddy from observations. As an example, Fig. 8 shows three snapshots of the velocity field: 20 min after the beginning of the first survey, at HW-1.2 h (Fig. 8a); at the end of the first survey, at HW+0.5 h (Fig. 8b); and at the end of the third survey, at HW + 2 h (Fig. 8c). As it can be seen, the OI method enables relatively accurate assessment of the circulation pattern. At the beginning of the period (HW-1.5 h), the eddy center was located just south of the harbour entrance, 300 m east of the western seawall, and its size appeared to be somewhat smaller than in Fig. 5a, but consistent with the aerial photo (Fig. 1, right panel) taken 1 h before the HW during mean tide conditions. Qualitative comparison of the right panel in Figs. 1 and 8a reveals a high degree of consistency between the remotely sensed circulation pattern and interpolated velocity field at the corresponding stage of tidal cycle (HW-1.5 h). The eddy occupies the southern and central parts of the BH, dominating over two thirds of the total area. In the northern part, the water inflow is observed with mean velocities ranging from 0.5 to 1 m/s. A part of this flow continues east-northward and leaves the harbour through a passage between the northern seawall and the coast. Later, (at HW+0.5 h), the eddy migrated northeastward and expanded in size to occupy the entire area of the harbour (Fig. 8b). 1.5 h later, the center of the eddy moved slightly northward with the currents directed out of the harbour on the eddy's western periphery, matching the ebb tide. The background color in Fig. 8 indicates the difference in the velocity magnitude between the space-time interpolated currents and the respective currents of the background model run. Most of the data-induced changes are observed in the northern part of the harbour with the major difference (≈0.30 m/s) at the periphery of the eddy, showing significant modifications of the circulation pattern provided by the interpolation.

During the second survey (LW-2H, on March 29), the evolution of the flow field was less prominent (results not shown). This is due to the relatively short duration of the survey (approximately 1.7 h), the weak current field, and the absence of rotational flow. The current pattern remained similar to that shown in Fig. 5b with minor variation of the magnitude. It did not exhibit any eddy-like features and resembled a typical outflow pattern with spatially homogeneous divergence.

3.5 Cross validation with bottom-mounted ADCP

To test the quality of interpolation and its ability to reproduce the time evolution of the flow field, the interpolated velocity series were compared with velocity records obtained by the bottom-mounted ADCP, which was deployed for 25 h between March 27 and 28, in the middle of the harbour entrance (black square in Fig. 1), 300 m east of the concrete caisson. The ADCP, installed on the bottom tripod (Searider of OceanScience), was recording velocities in the fast pinging mode (2 Hz) with the bin size of 0.4 m. Figure 9 shows meridional and zonal velocity components recorded by the ADCP. One can see that the strongest currents (>0.8 m/s) occur approximately 1.5 h before the HW with a clear dominance of the zonal velocity. Velocity profiles are nearly

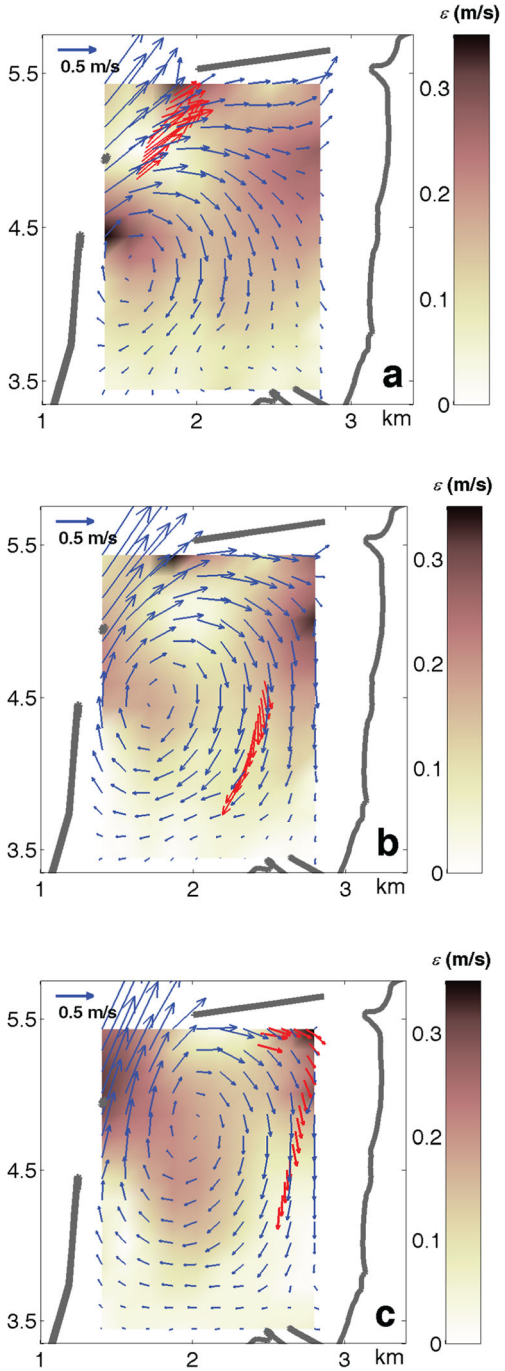

Fig. 8 Evolution of the transient anticyclonic eddy starting at HW-1.2 h (**a**) to HW+0.5 h (**b**) to HW+2 h (**c**). *Red arrows* show 30-s averaged ADCP velocities recorded along the track of surveys 1 and 3 for the respective tidal stages. *Blue arrows* show interpolated velocities. *Background shading* reflects the difference between the survey velocities interpolated in space and time and model velocities at mid-time of surveys 1 and 3 (shown in Fig. 6a, c)

homogeneous in the water column during the flood tide, with slightly decreasing velocity values towards the bottom and the surface. As already mentioned in Section 2.1, the ebb tide lasts longer than the flood tide, and the velocity evolution is characterized by a strong asymmetry.

The first survey (its period is shown by blue lines in Fig. 9) was conducted 2 h after the ADCP deployment. The velocities recorded by the bottom-mounted ADCP, approximately 1 m below the surface, the respective model velocities in the surface layer, and the interpolated velocities are shown in Fig. 10. The comparison demonstrates a good qualitative agreement between the ADCP and the model (correlation values $C=0.81$ and $C=0.87$ for zonal and meridional velocity components, respectively). A considerably better agreement is achieved for interpolated velocities ($C=0.97$ and $C=0.89$) derived from the survey measurements. In terms of the mean relative errors, the survey-derived velocities are characterized by almost two times lower values of e than velocities simulated by the model ($e=0.09$ and $e=0.17$, respectively). Moreover, a noticeable phase lag between the ADCP data and modeled zonal velocity (compare black squares and black line in Fig. 10) is effectively eliminated in the interpolated velocity series. These results provide a reasonable support for the validity of the proposed OI interpolation algorithm.

3.6 Interpolation errors

Accuracy of the velocity field reconstruction was estimated using the relationship (4) for the diagonal elements of a posteriori error covariance matrix that merges information available from the model and observations. The latter has a contribution from the instrumental error of velocity profiling (0.04 m/s for the ADCP configuration in use) and the representation error, ranging from 0.05 to 0.14 m/s, which accounts for velocity variations at time scales below 30 s (Fig. 3). The intensity of these sub-grid velocity fluctuations depends mainly on environmental variables (e.g., wind and wave effects), transect orientation with respect to the surface waves, and the speed of surveying. In general, surveying in the along wave direction provides lower rms errors (0.05–0.10 m/s). The model errors were estimated as the rms variation of the velocity field over the 14 ensemble members.

The towed ADCP observational uncertainties (0.07–0.15 m/s) are larger compared to the moored ADCP and HF radar current measurement uncertainties (e.g., Liu et al. 2014). However, the proposed technique provides a significant error reduction estimated as the ratio $\gamma=(\sigma^2(\boldsymbol{x})/\langle\mathrm{diag}\,\boldsymbol{B}\rangle)^{1/2}$ and varying in the range 0.3–0.6, which increases the confidence in velocity field reconstruction from ADCP measurements. Figure 11 shows a composite map of the error reduction ratio γ for the first survey. The numerator and denominator in the expression for γ were computed by time averaging over the 240 snapshots of the corresponding error fields. The values of γ appear to be somewhat larger near the exit and outside the Boulogne harbour due to larger modeling and observational errors in the regions of stronger currents. In the absolute values, the time-mean interpolation errors σ were 0.07, 0.03, and 0.06 m/s for the first, second, and third surveys,

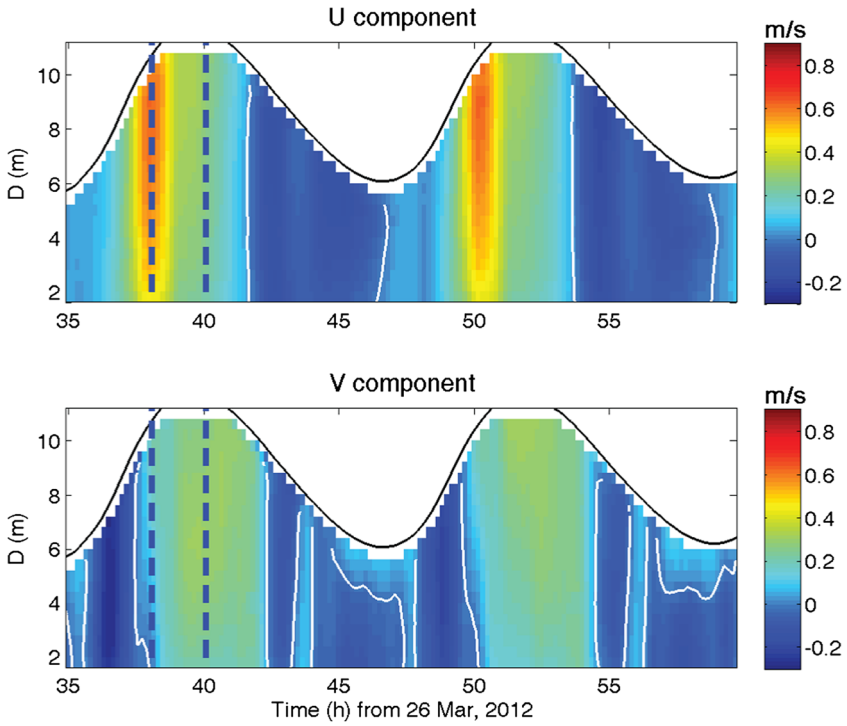

Fig. 9 Ten-minute averaged zonal (*above*) and meridional velocities measured by the bottom-mounted ADCP as functions of distance above the bottom. *White lines* match zero-velocity value. *Blue dashed lines* show the period of the first ADCP survey on March 27

respectively. This is significantly smaller than the estimated modeling and observation errors and consistent with the mean misfits shown in Table 1 (columns 4, 5 and 7, 8).

Inspection of the differences between the interpolated velocities and the ensemble-averaged model run indicates that the model slightly overestimates the northern inflow into the harbour and underestimates the circulation in the BLH interior (Fig. 8a). At the start of the first survey, the inflow is disturbed by a caisson located in the middle of the harbour entrance, producing an extra clockwise vorticity. By the end of the survey, the velocity difference becomes small (0.03–0.06 m/s) all over the domain (Fig. 8b), with an exception of the 0.06–0.10 m/s overestimation of the northern inflow. Similar behavior has been diagnosed for the third survey (Fig. 8c) and (to a lesser extent) second survey. Such error structure of the flow field near the BLH entrance can partly be explained by the presence of the "concrete caisson" (10 × 10 m), not resolved by the model grid, whose impact on the circulation is clearly visible during the inflow phase of the tidal cycle.

4 Discussion and conclusions

Due to the growing interest in tidal energy conversion technique worldwide (Black and Veatch 2005), and in the northwestern European shelf seas in particular (e.g., Lewis et al. 2015), a detailed assessment of the natural resource is required to determine commercial viability of any project prior to device deployment. Underway vessel-mounted ADCP observations are especially efficient for monitoring of the tidal flows and computing the energy fluxes through the channels in tidally dominated basins

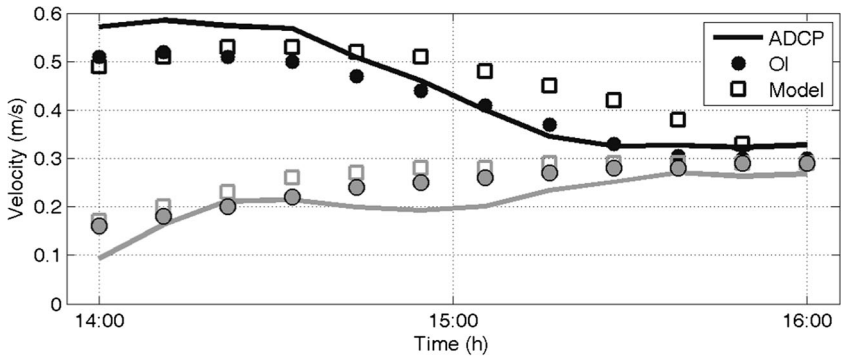

Fig. 10 Zonal (*black*) and meridional (*gray*) velocity components observed by the bottom-mounted ADCP (*solid line*), simulated by the model (*squares*), and derived from the interpolated (OI) survey data (*black circles*) in a grid point closest to the ADCP location

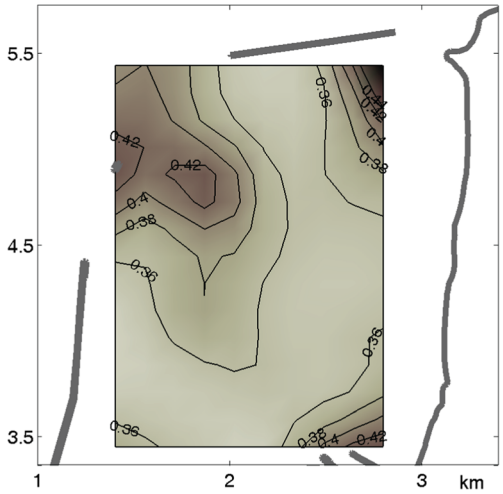

Fig 11 A composite map of the error reduction γ for the first survey

(Fairley et al. 2013). The transect time is a well-known limitation of vessel-based surveying compared to bottom-mounted instrumentations. To avoid distortion of the results caused by temporal variation of the tidal flow during the survey, very short (20–30 min) transects are repeatedly made, usually around the peak tidal flow (e.g., Evans et al. 2015). The respective spatial patterns of power density suffer from the lack of consistency due to noise in the data and to temporal variation of the flow. This time limitation prevents continuous studies of larger domains which require surveying times comparable with the characteristic time scale of the velocity field (T~2–4 h).

The end goal of the surveying of any area under tidal influence is to assess the velocity field evolution. It can be achieved through accurate space-time interpolation of the survey data recorded at high spatial resolution. The efficiency of such interpolation is based on tight spatial and temporal correlations of the velocity field within the tidal cycle. In their recent study, Goddijn-Murphy et al. (2013) showed that if a tidal model provides a reasonable estimate of flow field, an output of the model could be utilized to project the transect data to a fixed (central) time of the survey. Using a 2D model POLPRED (Proudman Oceanographic Laboratory Model), they performed a reasonably accurate synchronization of the velocity data to the mid-survey time. However, a relatively coarse resolution of the model did not allow assessing smaller-scale features of the tidal flow, such as eddies, cross currents, and jets, while temporal resolution of the model (10 min) appeared to be close to the limit required for resolving rapid evolution of these features. It should be mentioned that the majority of oceanographic vessels operating in coastal regions are equipped with an ADCP, and availability of a technique for calculating virtual snapshots of the velocity field from the underway velocity measurements is an important issue.

The present study has two objectives. First, we present a low-cost, compact, experimental platform for underway current profiling. The towed system has several advantages over vessel-mounted ADCP: (a) it offers a possibility of profiling at low depth (up to 2 m, for example), (b) it is not intrusive and does not disturb the flow especially in the surface layer, and (c) it provides increased accuracy of velocity and bottom tracking (due to small disturbances of the ADCP mounted on freely floating frame, than installed on a big boat).

The platform can be easily upgraded to a multi-sensor observing system by installing additional instruments such as the Acoustic Doppler Velocimeter (ADV) for velocity recording near the water surface and a micro-CTD for underway measurements of temperature, salinity, oxygen concentration, fluorescence, and other quantities. Another advantage of the system is that it does not require cable connection to the on-board computer for data acquisition. The data are recorded and stored in the instruments during the survey.

Second, we extend the approach of underway velocity profiling by employing the optimal interpolation technique in both space and time to retrieve the entire evolution of tidal currents from the survey data. The technique employs tight space-time correlations in the tidal flow field that can be accurately simulated by the existing state-of-the-art numerical models.

Three test surveys were performed in the Boulogne harbour (Opal coast of France). Results of the testing indicate that tidal circulation in limited domains (starting from 1 × 1 km) can be accurately reconstructed from underway ADCP data acquired by a single towed platform capable of surveying at speeds up to eight knots (4 m/s) under moderate wave conditions. The result is obtained by blending filtered observations with the output of a numerical model in the framework of optimal interpolation of the data in both space and time. The utilized MARS-3D model provided the first guess (background) evolution of the velocity field in the study area which was then corrected by the data. The proposed space-time interpolation algorithm explicitly takes into the account both observational and modeling errors, and the latter was derived from the statistics of a longer model run executed in the area prior to the survey.

Due to the high resolution of measurements and the model grid, the interpolated velocity fields capture all the key features of circulation in the BH, such as rapidly evolving transient eddy, tidal jet at the harbour entrance, and diffuse flow in the shallow regions during the ebb tide.

The quality of the currents' reconstruction was validated in two ways: against the mean tide model run and against independent bottom-mounted ADCP data. Both tests demonstrated significant (30 to 60 %) reduction of the model-data misfit for the velocity field obtained as a result of space-time interpolation. Good correspondence between the interpolated surface velocities and velocities observed by the bottom-mounted

ADCP 1 m below the surface indicates an interesting possibility of reconstructing the entire 3D evolution of the velocity field within the tidal cycle by blending the vertical velocity profiles obtained during the survey with the model output. This extension of the interpolation algorithm would require consistent representation of the boundary layer physics and frictional effects by the model as well as availability of an improved high-resolution bathymetry. We believe, however, that the presented synthesis of the surface velocity observations with the model output does already provide a significant improvement in the underway tidal velocity surveying in terms of both the decreased discrepancy and better correlations with independent observations.

The presented low-cost current mapping system can be seen as complementary to other coastal observing systems, such as HF radars and moored ADCPs. The former has an advantage of high temporal (~20 min) and spatial (0.5–1 km) resolution. However, the noise level for radial velocity measurements by a radar can reach 0.08 m/s (Forget 2015). Limitations related with the sea state and the presence of islands and headlands can increase the observation error or considerably decrease the amount of the available data in some sectors of a radar coverage zone. Despite somewhat lower accuracy (0.10–0.15 m/s) of a towed ADCP system compared to HF radars, it has a capability of measuring subsurface currents, while the proposed interpolating algorithm reduces the observation error by up to 60 %, thus increasing the accuracy of the reconstructed velocity field. We believe that the proposed current mapping system may advance understanding and assessing coastal circulation in tidal environments, especially when used in combination with moored ADCP and/or HF radar velocity observations.

Further development of the system could be done in several directions. An important issue is an improvement of the numerical model, whose performance is crucial for the space-time interpolation of the survey data, especially in the case of 4D interpolation. In that respect, utilizing the water depth data acquired by the presented surveying system is essential for accurate mapping of the seafloor and for enriching the interpolation algorithm by information on SSH variability. Additional data from local tidal gages can also be used to improve the quality of the survey processing. Another interesting possibility involves processing the suspended particle concentration also recorded by the experimental system. Combining these records with the reconstructed velocity field and the passive tracer transport model, it might be possible to obtain estimates of the suspended matter dynamics, which is very important in many applications.

The presented mobile surveying system has been successfully tested in several shallow water (5–25 m) tidal basins including the Dover harbour and (non-tidal) Gulf of Lyon (Barbin et al. 2014) and demonstrated good performance at towing speeds up to 4 m/s. The system is equipped with a relocatable numerical model (MARS) which allows efficient space-time interpolation of the survey data at high resolution in ports and estuaries. Due to the hardware portability (Section 2.2), the system is fast in deploying and providing surveillance results at the expense that is significantly below the typical cost of ADCP surveying from larger vessels. The proposed low-cost mobile surveying system can also be considered as a good complement to larger stationary coastal ocean observing systems (e.g., Liu et al. 2015) and could be efficiently applied in marine energy resource assessments as well as in more general coastal research. In particular, the system can be effectively used for detailed studies of the tidal stream preceding to deployment of reduced-scale and full-scale tidal turbines (aiming precise positioning and optimization of the tidal energy production) for studies of the impact of tidal turbines on local circulation, turbulence, sediment dynamics, and for other applications which require full tidal cycle surveying at fine resolution.

Acknowledgments The authors would like to acknowledge the support of the Interreg IVB (NW Europe) "Pro-Tide" Program and support from the US Office of Naval Research. The skill and experience of skipper Eric Lecuyer and his help during the fieldwork are appreciated and acknowledged. We also thank two anonymous reviewers for their valuable comments on the manuscript.

References

Barbin Y, Bellomo L, Doglioli A, Forget P, Fraunié P, Lecuyer E, Malengros D, Marmain J, Molcard A, Petrenko A, Quentin C, Sentchev A (2014) Experimental investigation of the relationship between HF radar measurements of currents and the dynamical properties of the upper ocean. Geophys Res Abstr 16. EGU2014-13078, EGU General Assembly

Barth A, Alvera-Azcárate A, Beckers J-M, Weisberg RH, Vandenbulcke L, Lenartz F, Rixen M (2009) Dynamically constrained ensemble perturbations: application to tides on the West Florida Shelf. Ocean Sci 5:259–270

Black and Veatch (2005) Tidal stream energy resource and technology summary report. Carbon Trust

Blunden LS, Bahaj AS (2006) Initial evaluation of tidal stream energy resources at Portland Bill, UK. Renew Energy 31:121–132

Bretherton FP, Davis RE, Fandry CB (1976) A technique for objective analysis and design of oceanographic experiments applied to MODE-73. Deep Sea Res 23:559–582

Candela J, Beardsley RC, Limburner R (1992) Separation of tides and sub-tidal currents in ship-mounted acoustic Doppler current profiler observations. J Geophys Res 97:769–788

Evans P, Mason-Jones A, Wilson C, Wooldridge C, O'Doherty T, O'Doherty D (2015) Constraints on extractable power from energetic tidal straits. Renew Energy 81:707–722

Fairley I, Evans P, Wooldridge C, Willis M, Masters I (2013) Evaluation of tidal stream resource in a potential array area via direct measurements. Renew Energy 57:70–78

Forget P (2015) Noise properties of HF radar measurement of ocean surface currents. Radio Sci 50(8):764–777

Gandin LS (1963) Objective analysis of meteorological fields. Gidrometizdat (GIMIZ), Leningrad (translated by Israel Program for Scientific Translations, Jerusalem, 1965, 238 pp.)

Geyer WR, Signell R (1990) Measurements of tidal flow around a headland with a shipboard acoustic Doppler current profiler. J Geophys Res 95:3189–3197

Goddijn-Murphy L, Woolf DK, Easton M (2013) Current patterns in the inner sound (Pentland Firth) from underway ADCP data. J Atmos Oceanic Tech 30(1):96–111

Gooch S, Thomson J, Polagye B, Meggitt D (2009) Site characterization for tidal power. In OCEANS 2009, MTS/IEEE Biloxi-Marine Technology for Our Future: Global and Local Challenges 1–10

Haas KA, Fritz HM, French SP, Smith BT, Neary V (2011) Assessment of energy production potential from tidal streams in the United States. Available online at http://energy.gov/sites/prod/files/2013/12/f5/1023527.pdf

Hamill TM, Whitaker JS, Snyder C (2001) Distance-dependent filtering of background error covariance estimates in an ensemble Kalman filter. Mon Weather Rev 129:2776–2790

Holdaway MR (1996) Spatial modeling and interpolation of monthly temperature using kriging. Climate Res 6:215–225

Jouanneau N, Sentchev A, Dumas F (2013) Numerical modelling of circulation and dispersion processes in Boulogne-sur-Mer harbour (Eastern English Channel): sensitivity to physical forcing and harbour design. Ocean Dyn 63:1321–1340

Kalnay E (2002) Atmospheric modeling, data assimilation and predictability. Cambridge University Press

Lazure P, Dumas F (2008) An external–internal mode coupling for a 3D hydrodynamical model for applications at regional scale (MARS). Adv Water Resour 31:233–250

Lewis M, Neill SP, Robins PE, Hashemi MR (2015) Resource assessment for future generations of tidal-stream energy arrays. Energy 83:403–415

Li C, Armstrong S, Williams D. Residual eddies in a tidal channel. Estuar Coasts 29:147–158

Liu Y, Weisberg RH, Merz CR (2014) Assessment of CODAR and WERA HF radars in mapping currents on the West Florida Shelf. J Atmos Oceanic Tech 31:1363–1382

Liu Y, Kerkering H, Weisberg RH (Eds) (2015) Coastal Ocean Observing Systems, Elsevier

MacMahan J, Vennell R, Beatson R, Brown J, Reniers A (2012) Divergence-free spatial velocity flow field interpolator for improving measurements from ADCP-equipped small unmanned underwater vehicles. J Atmos Oceanic Tech 29(3):478–484

Neill SP, Hashemi MR, Lewis MJ (2014) The role of tidal asymmetry in characterizing the tidal energy resource of Orkney. Renew Energy 68:337–350

Old CP, Vennell R (2001) ADCP measurement of the velocity field of an ebb tidal jet. J Geophys Res 106:7037–7050

Plus M, Dumas F, Stanisière J-Y, Maurer D (2009) Hydrodynamic characterization of the Arcachon Bay, using model-derived descriptors. Cont Shelf Res 29:1008–1013

Quirapas, MA, Lin, H, Abundo, M, Brahim, S, Santos D (2015) Ocean renewable energy in Southeast Asia: a review. Renew Sust Energ Rev 41:799–817

Simpson JH, Mitchelson-Jacob EG, Hill AE (1990) Flow structure in a channel from an acoustic Doppler current profiler. Cont Shelf Res 10:589–603

Thiébaux HJ, Pedder MA (1987) Spatial objective analysis with applications in atmospheric science, vol 1. Academic, London

Vennell R (1994) Acoustic Doppler current profiler measurements of tidal phase and amplitude in Cook Strait, New Zealand. Cont Shelf Res 14:353–364

Vennell R (2006) ADCP measurements of momentum balance and dynamic topography in a constricted tidal channel. J Phys Oceanogr 36:177–188

Vennell R, Beatson R (2006) Moving vessel acoustic Doppler current profiler measurement of tidal stream function using radial basis functions. J Geophys Res 111:C09002. doi:10.1029/2005JC003321

Vennell R, Beatson R (2009) A divergence-free spatial interpolator for large sparse velocity data sets. J Geophys Res 114:C10024. doi:10.1029/2008JC004973

Weisberg RH, Liu Y, Merz CR, Virmani JI, Zheng L (2012) A critique of alternative power generation for Florida by mechanical and solar means. Mar Technol Soc J 46(5):12–23. doi:10.4031/MTSJ.46.5.1

Wunsch C (1996) The ocean circulation inverse problem. Cambridge University Press